Soft Matter

PAPER

View Article Online
View Journal | View Issue

Cite this: *Soft Matter*, 2014, **10**, 6219

Rheology and simulation of 2-dimensional clathrin protein network assembly†

Jules J. VanDersarl,[ac] Shafigh Mehraeen,[b] Alia P. Schoen,[ac] Sarah C. Heilshorn,[ac] Andrew J. Spakowitz[bc] and Nicholas A. Melosh*[ac]

Received 6th January 2014
Accepted 17th June 2014

DOI: 10.1039/c4sm00025k

www.rsc.org/softmatter

Clathrin is a three-legged protein complex that assembles into lattice structures on the cell membrane and transforms into fullerene-like cages during endocytosis. This dynamic structural flexibility makes clathrin an attractive building block for guided assembly. The assembly dynamics and the mechanical properties of clathrin protein lattices are studied using rheological measurements and theoretical modelling in an effort to better understand two dynamic processes: protein adsorption to the interface and assembly into a network. We find that percolation models for protein network formation are insufficient to describe clathrin network formation, but with Monte Carlo simulations we can describe the dynamics of network formation very well. Insights from this work can be used to design new bio-inspired nano-assembly systems.

Introduction

Nature creates a remarkable array of functional nanostructured architectures through self- and guided- assembly. The fidelity inherent in biological assembly is attractive for a broad range of applications, including inorganic/organic materials based on biopolymer assemblies composed of DNA,[1–4] proteins,[5–8] bacterial membranes,[9–12] and virus particles.[13–21]

Clathrin proteins are a fascinating system for examining biological assembly since these flexible units can adopt diverse structures ranging from 2-dimensional hexagonal arrays[22] to 3-dimensional shell-like structures.[23–25] Clathrin is a major player in endocytosis and exhibits highly dynamic behaviour within the cell, which potentially could be harnessed to create materials with temporally tunable properties. The variety of nanostructures possible from this single subunit also makes it an ideal system to study the kinetic and thermodynamic driving forces that lead to assembly of specific nanoscale structures. Dynamic control over assembly and reorganization could potentially be extended to localized regions or vary over time, opening the door for a new class of biotemplate engineered structures featuring tunable designs and active functionalities.

Characterization of clathrin protein flexibility[26,27] and cage assembly[28,29] has been examined with optical[26,27] and X-ray[30] techniques. However, large area clathrin networks have proven more difficult to study. Spanning 2-dimensional clathrin assemblies are formed *in vivo* on the cell membrane surface in the early steps of endocytosis.[31] *In vitro*, similar 2-dimensional network formation can be recreated on lipid monolayers at air–water interfaces, and have been observed using transmission electron microscopy.[22,32] However, these static measurements miss the rich kinetics of clathrin absorption, recruitment, and assembly, which have recently proven more dynamic than previously thought.[33]

While clathrin network assembly is complex, two of the critical steps are: (1) individual clathrin triskeles binding to PIP_2 (phosphatidylinositol 4,5-bisphosphate) lipids *via* an adaptor protein,[34] and (2) protein migration and self-association to form the hexagonal network. During large area network formation, these two steps largely occur simultaneously. Therefore, in order to properly study clathrin network assembly one must be able to separately measure and quantify both clathrin adsorption and organization. Further environmental factors such as protein concentration, pH, and salt concentration must also be controlled.[28]

Mechanical measurements are an effective means of monitoring such network formation *in situ*, as the surface pressure and mechanical modulus are highly sensitive to the number density and intermolecular attachment of the individual units, respectively. Surface rheological techniques have been used to monitor protein assemblies at air–water interfaces, and have the potential to distinguish between different degrees of organization and defect density within the network with appropriate modelling.

Here we present rheological measurements of clathrin recruitment and assembly together with mathematical percolated network models and Monte Carlo simulations to estimate

[a]*Materials Science & Engineering, Stanford University, Stanford, CA 94305, USA. E-mail: nmelosh@stanford.edu*

[b]*Chemical Engineering, Stanford University, Stanford, CA 94305, USA*

[c]*Stanford Institute for Materials and Energy Science, SLAC National Accelerator Laboratory, Menlo Park, CA 94025, USA*

† Electronic supplementary information (ESI) available. See DOI: 10.1039/c4sm00025k

the quality and quantity of clathrin assemblies in real time. These results reveal that traditional percolation models are insufficient to describe clathrin networks, but a Brownian dynamics model accounting for molecular properties describes network growth well. Greater understanding of clathrin assembly under various conditions may allow better shape and kinetic control, offering a new and powerful platform for engineering nano-assembly systems.

Results and discussion

Network formation was measured from the mechanical properties of clathrin assembling onto a lipid monolayer at an air–water interface using interfacial shear rheometry (ISR). ISR is simultaneously sensitive to two different surface properties, the surface pressure (N m^{-1}) and surface modulus (N m^{-1}), which relate to the concentration of clathrin on the lipid and the degree of clathrin crosslinking, respectively. Through modeling, the measurements can be separated into these individual components, allowing a clear view into the steps of network formation.

Experiments were conducted with a Langmuir monolayer of lipids as a model for the cytosolic cell membrane surface.[35] Using a Langmuir–Blodgett trough or a Teflon dish, a mixture of lipids and cholesterol meant to approximate a cell membrane (20% PIP_2, 35% SOPC, 35% SOPE, and 10% cholesterol) were dissolved in solvent (0.1 mg ml^{-1} in chloroform–methanol–water at 20 : 9 : 1 v/v) and spread on a buffered subphase (HKM buffer, 25 mM Hepes pH 7.4, 125 mM potassium acetate, 5 mM magnesium acetate, 1 mM dithiothreitol), in accordance with protocols previously described elsewhere.[32] Lipids were spread dilutely onto the liquid surface on the Langmuir trough, and compressed to an initial surface pressure of 10 mN m^{-1}. Experiments were performed at constant surface area. After the lipids reached a stable surface pressure (little or no surface pressure drift), clathrin molecules ($\sim$1 mg ml^{-1} plus associated adaptor proteins in HKM buffer) were injected into the subphase. These clathrin proteins were derived from bovine clathrin coated vesicles, and included their associated adaptor proteins. The subphase was stirred gently to promote clathrin motion without perturbing the lipid surface, increasing binding kinetics and minimizing experimental drift. After injecting a mixture of clathrin and adaptor protein into the subphase, the proteins begin binding to the PIP_2 lipids in the monolayer, increasing both the surface pressure and surface modulus. The surface pressure was measured using a Wilhelmy plate of either filter paper or platinum, while the surface modulus was measured with an ISR. The ISR consisted of a Langmuir–Blodgett trough with a pair of Helmholtz coils and a camera as previously described.[36,37] A magnetized needle, placed at the air–water interface, was oscillated back and forth using a magnetic field, while the movement of the needle was recorded with the camera. By observing the magnitude and phase of the needle oscillation in relation to the magnetic field oscillation the surface moduli of the interface can be determined. The needle oscillates in an open-ended glass channel, which creates well defined shear fields, and makes the data obtained fully quantitative. Unless otherwise specified, the ISR probing frequency and magnitude was 0.1 Hz and 0.5% strain, respectively.

The surface pressure of the lipid surface increased as a function of clathrin concentration in the subphase, Fig. 1. Protein binding to a lipid monolayer increases the surface pressure in proportion to the concentration of bound protein.[38] This can be described by a Langmuir adsorption isotherm for ideal binding, or the Hill equation for molecules which undergo cooperative binding, such as clathrin. Fitting a Hill equation to our data yields a disassociation constant for the clathrin–lipid interaction, which was found to be 1.6×10^{-10} M, a typical value for protein–ligand interactions, and a Hill coefficient of $n = 1.5$ (Fig. 1). This shows positive cooperative binding, but the Hill coefficients derived in our study were consistently smaller than others found for clathrin assembly *in vivo* ($n \sim 3$).[39] However, since Hill coefficients are very sensitive to pH, salt, and temperature, variation between the *in vivo* and *in vitro* conditions may lead to different coefficients. Additionally, as our *in vitro* environment contains only lipids, clathrin, and adaptor proteins, it is also possible that our experiment lacks some biological species that would synergistically increase the cooperative magnitude of binding.[39]

As the surface concentration of clathrin triskelia increases, they will begin to attach to each other and form 2-D protein networks. As these networks grow larger and more interconnected, the surface modulus of the Langmuir film increases. Fig. 2 shows the elastic storage modulus as a function of time after injection of 100 nM of clathrin into the subphase. The modulus increases monotonically over 4 hours, after which evaporation and oxidative effects degrade the experiment. Clathrin injected under a lipid layer without the clathrin-binding lipid PIP_2 does not increase the surface modulus (Fig. 2), demonstrating that the increase in surface modulus is not due to non-specific protein adsorption or interaction, but rather specific clathrin–lipid binding.

In order to minimize the effect of the lipids on the surface modulus, we used only unsaturated lipids with a transition temperature below 20 °C (SOPC, 1-octadecanoyl-2-(9*Z*-octadecenoyl)-*sn-glycero*-3-phosphocholine, and SOPE, 1-octadecanoyl-2-(9*Z*-octadecenoyl)-*sn-glycero*-3-phosphoethanolamine). This prevents a lipid gel phase, which exhibits both a higher

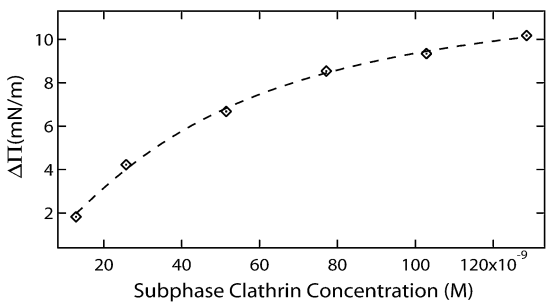

Fig. 1 Clathrin–lipid binding affinity upon serial injection of clathrin into the subphase. Experimental surface pressure measurements (diamonds) are fit (dashed line) to the Hill equation.

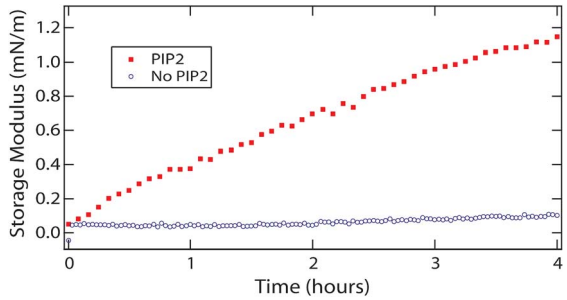

Fig. 2 Only lipid monolayer films with PIP_2 show a modulus increase after clathrin is injected into the subphase.

modulus and a strong phase transition during compression. Furthermore, unsaturated lipids prevented phase separation of the PIP_2, ensuring a homogenous lipid monolayer.[40]

Fig. 3 shows the rise in surface modulus for a pure lipid monolayer during compression (pressure-area isotherm), and during clathrin binding (constant surface area). Clathrin binding alone causes the surface pressure to rise to almost 15 mN m^{-1}. Over this surface pressure range the modulus of the pure lipid film increased slightly above 10 mN m^{-1} (Fig. 3). This small increase indicated the increased modulus is almost entirely (>97%) from the clathrin network, and the lipid component is neglected in the remainder of the paper.

Even without forming well-ordered, spanning networks, the surface adsorption of surface active polymers is known to require a critical concentration before inducing moduli changes.[41] This produces a modulus increase behaviour similar to percolation network formation. However, this is not due to bonding between polymer clusters, but due to packing effects. Isolated, non-interacting clusters can also increase the surface moduli, but only at high frequencies.[42] At lower frequencies, the clusters can rearrange themselves quickly enough to dissipate any energy that would affect a modulus increase. Only as the clusters begin to pack against each other do changes occur in the low frequency or quasi-static moduli. We do see some evidence of these changes during network formation and growth, as the modulus seems to grow a little faster when measured at higher frequencies (Fig. S1†). Because of these possible artifacts, we measured network formation at very low frequencies (0.1 Hz), ensuring that the measured modulus increase was from the formation of stable, long-term bond formation between smaller networks, and not from transient connections. The use of slow, quasi-static, measurements also allowed for better comparison to conventional elastic modulus data. Once the network is well-formed, the modulus was invariant with measurement frequency (Fig. S2†), which is consistent with a temporally robust network with stable bonds.

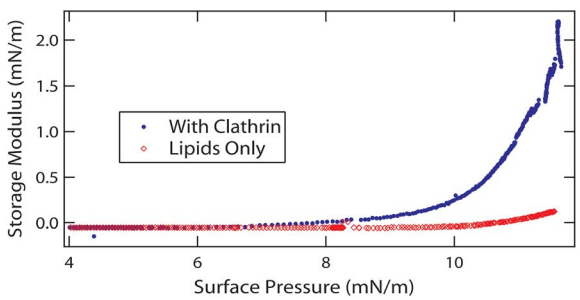

Fig. 3 The surface modulus of a lipid film with bound clathrin proteins is much larger than that of lipid only films at comparable surface pressures.

In sum, these data show that the clathrin binding to the lipid surface greatly increases the surface modulus, and does so in a manner suggesting a percolation network. Furthermore, the network structure is dominated by stable bond formation between clusters, and not simply by packing effects. However, the nature of clathrin network is unclear at this point. A true percolation network assumes non-interacting species and random site occupancy, while previous work shows that localized clathrin recruitment coordination[39] and surface clustering occurs.[22,32]

In order to better understand the nature of clathrin network interaction, we developed two models to compare against the experimental data, one based on a random percolation network, and the other based on a combined Monte Carlo and Brownian dynamics simulation that accounts for clathrin clustering with molecular diffusion, binding, and unbinding events.

In the first percolation model, changes in moduli at low, quasi-static frequencies can only occur when site occupancy rises above a critical threshold. The mechanical strength of a network above the critical percolation concentration increases following a power law relation.[43] From this relation, we can estimate the shear strength of a percolation network at site occupancy values above the percolation threshold as:

$$G = G_{\max} A(\rho - \rho_c)^b, \quad (1)$$

where A and b are 8.38 and 1.98, respectively, for hexagonal bond networks in shear,[44] with a critical percolation density, ρ_c, for a hexagonal bond network of 0.6527.[45] Here $G_{\max}$ is the shear modulus of a perfect hexagonal network, and ρ is the site occupancy.

Site occupancy was determined from the rise in surface pressure after protein injection, and surface modulus measured using ISR.

For the ISR experiments, the lipid monolayer was spread on the liquid surface and compressed to 10 mN m^{-1}. Then an excess of clathrin (1 mM) and adaptor proteins were injected into the subphase and gently mixed continuously with a peristaltic pump. Within a few minutes of protein injection, the surface pressure began to rise, while the surface modulus did not begin to increase for almost an additional hour (Fig. 4a), indicating protein adsorption but without formation of a percolating path. Adapting eqn (1) for ISR experiments results in

$$G_{\text{total}} = G_{\text{lipids}} + G_{\text{clathrin}}\left[A\left(\frac{\Delta\pi}{\Delta\pi_{\max}} - \rho_c\right)^b\right] \quad (2)$$

in this equation, A, b, and ρ_c are mathematically derived percolation constants, and remain unchanged from eqn (1). $\Delta\pi$

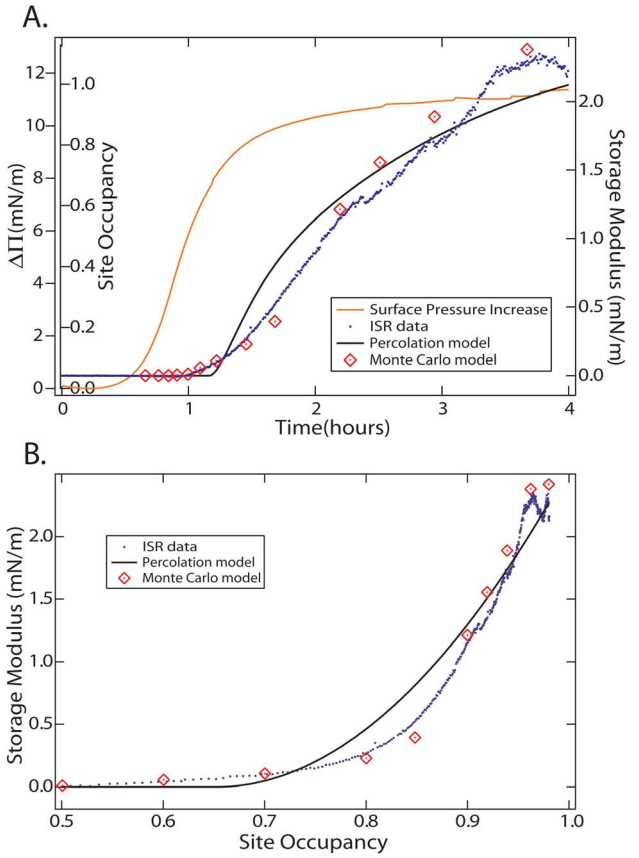

Fig. 4 (A) ISR measurements of surface pressure change over time (orange curve, left axis) and surface modulus *vs.* time (blue dots, right axis). The orange curve is used to calculate site occupancy at each point during the experiment (second left axes), which is then used in calculations for the percolation model for network strength (black curve), and the Monte Carlo simulated effective modulus of the network (red diamonds). (B) Contains the same data and models, but is plotted as a function of site occupancy. Monte Carlo data is for $\rho \sim$ 0.10, 0.20, 0.30, 0.40, 0.50, 0.60, 0.70, 0.80, 0.85, 0.90, 0.92, 0.94, 0.96, and 0.98.

is the rise in surface pressure after protein injection (Fig. 4a, orange line), and $\Delta\pi_{max}$ is the estimated rise in surface pressure if the experiment was allowed to proceed indefinitely. This value is estimated by fitting a double exponential to the surface pressure data and is estimated to be 12.25 mN m^{-1}. We assume this value represents complete site occupancy, as compared to previous work[32] we used an excess of PIP_2 in the monolayer and injected an excess of protein into the subphase. Therefore, we used $\Delta\pi/\Delta\pi_{max}$ to represent the site occupancy. The shear modulus for a lipid only interface, G_{lipids}, is approximately zero (Fig. 3), and was neglected. $G_{clathrin}$ is the shear modulus of a perfect clathrin network, which was not able to be accurately estimated from the ISR data (Fig. 4, blue dots). Attempts to estimate $G_{clathrin}$ by fitting curves to contiguous parts of the data suggest a possible range for the maximum modulus between 2.3 and 3.3 mN m^{-1}. We used 2.5 mN m^{-1} in Fig. 4 (black line), consistent with our hybrid Monte Carlo and Brownian dynamics simulation results. The effects other values of $G_{clathrin}$ have on the percolation model are shown in Fig. S3,† but they do not change the general shape or trend of the model, and thus do not affect any of our analyses or conclusions.

The results of this analysis are shown in Fig. 4. Below the critical percolation value, the modulus is zero. At p_c ($\Delta\pi \sim 8$ mN m^{-1}), the percolation model modulus rises sharply, before approaching the modulus of a perfect network. The data and models plotted in Fig. 4a as a function of time are plotted in Fig. 4b as a function of site occupancy, which is a more conventional way to view percolation data, and plots the simulation data against their independent variable. As the simulation data have no long-term temporal component, they are positioned on the abscissa in Fig. 4a such that the simulation and rheology data at each timepoint have equal site occupancy.

Following clathrin injection, the surface pressure began to rise at the 14.5 minute mark (Fig. 4a), while critical site occupancy (65.27%) occurs at the 70 minute mark, 55 minutes after the lipid surface pressure began to rise. At this point, the percolation model predicts the surface modulus should begin to rise (Fig. 4a, black). However, the ISR data shows the modulus begins to increase at the 61 minute mark (Fig. 4a, blue dots). Although this is only 9 minutes before the percolation model predicted, the site occupancy at this point is calculated to be only 55% (Fig. 4b, blue dots). However, the most dramatic difference between the percolation model and the empirical ISR data is in the shape and initial behavior of the increasing modulus. The pure percolation model predicts the surface modulus would rise sharply, while ISR data shows a much more gradual increase. The percolation model follows the overall behaviour reasonably, however misses the initial assembly period and the shape. These differences illustrate some shortcomings in the percolation model, which makes several simplifying assumptions and does not consider clathrin recruitment, coordination, reorganization, or grain boundaries between clathrin clusters.

In order to account for the clathrin assembly details ignored in the pure-percolation model and gain molecular-level insight into the measured modulus, we developed a coarse-grained clathrin model[46] that accounts for molecular flexibility and the dynamics of binding/unbinding of legs within the lattice.

We simulate the clathrin lattice in 2 dimensions, ignoring out-of-plane motion that would lead to domes and cages. Assembly at the air–water interface involves interfacial tensions that exceed membrane tensions by several orders of magnitude. Therefore, we assume the out-of-plane motion of the lattice is negligible to the overall structure and mechanical properties. However, our model is amenable to addressing such effects.[47] Using Monte Carlo and Brownian dynamics simulations, this model is capable of predicting large-scale mechanical properties while accounting for rearrangements in the lattice consistent with the observed clathrin network properties.

Several models have been developed to address a broad range of physical processes involving clathrin. Such models capture the structure of the clathrin triskelion and interactions between triskelia using patchy particles,[48] rigid triskelia with specific orientational interactions,[49] rigid triskelia with specific orientation interactions and varying pucker angle,[50] and triskelia composed of patchy particles with orientational

interactions and flexibility.[51,52] In comparison, our model does not include many of the details in the clathrin representation that were the focus of these studies.

Our approach in modeling these experiments is to use the simplest possible model with physical parameters that are set by separate experiments. In so doing, our model has only one floating parameter that is used to set the maximum storage modulus (see discussion below). The experiments occur over 4 hours in time, which is orders of magnitude larger than can be achieved by typical molecular simulation approaches. Thus, we perform a quasi-equilibrium assessment of the network elastic properties at varying occupancy to provide a bridge between the time-dependent experiments and the equilibrated coverage and network structure.

In our model, the clathrin triskelion is described as a three-legged hub (leg length of 24 nm) that is capable of forming bonds with neighbouring triskelia. Bond formation occurs with binding affinity ε that captures the favorable interactions between the clathrin protein legs. Bonded legs resist stretching and angles between bonded legs withstand bending deformation, which is captured by harmonic springs with stretching modulus κ_s and bending modulus κ_b (Fig. 5a). Equilibrium configurations are found using Monte Carlo simulations[53] followed by Brownian dynamics simulations to address the dynamics of assembly and reorganization.[46] A detailed discussion of the bending, stretching, and binding energies is found in Appendix A of ref. 46. The formulation of the Brownian dynamics simulations incorporates a dynamic Monte Carlo component for binding and unbinding processes which ensures thermodynamic equilibrium in the long-time limit. A single frequency parameter was chosen that is consistent with the local diffusion time of monomer motion, and is discussed in detail in Appendix B of ref. 46. These parameters were chosen in a way that allows for quasi-static study of the system.

Our computer simulation does not dynamically add clathrin triskelia to the system in a way that mimics adsorption to the lipid monolayer, rather, we preform clathrin assembly at various discrete densities in order to predict the effective storage modulus of clathrin networks at equivalent time points. For a given density the Monte Carlo simulations are initiated from a patch of perfect honeycomb lattice embedded in a periodic simulation box of 648 nm. Each Monte Carlo simulation is run for 2×10^7 steps. The binding affinity is set to $\varepsilon = 5.5$ k_BT, where k_B is Boltzmann constant and T is the temperature. One step of Monte Carlo simulation involves random selection of a pinwheel, moving it to a random position and making or breaking a bond of that pinwheel if possible. The binding and unbinding events are captured by a dynamic Monte Carlo algorithm embedded in the Brownian dynamics simulation.[46] In this approach, the pinwheel orientation is defined by its bonds. An unbound pinwheel is assumed to undergo rapid rotational diffusion in comparison to the time scale of bond formation. This assumption only affects fully unbound pinwheels, which are extremely rare in our simulations. Furthermore, our calculations of the mechanical properties of the lattice are unaffected by such dynamic issues.

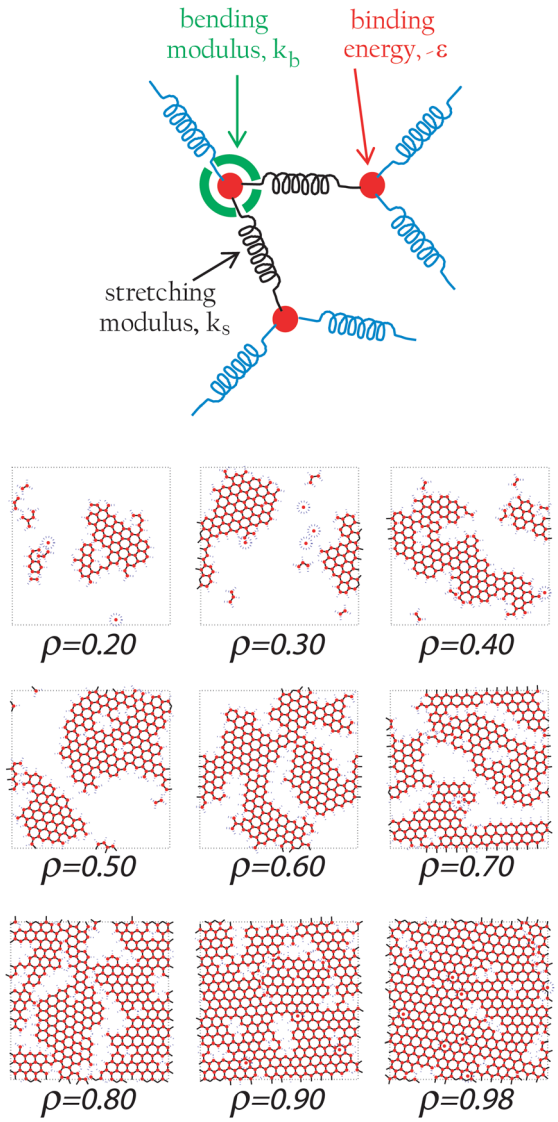

Fig. 5 Top panel: pinwheel model overview representing clathrin interactions. Bottom panel: snapshots are taken from Brownian dynamics simulations after 2000 time steps at various site occupancy densities.

After each Monte Carlo simulation a Brownian dynamics simulation starting from the final Monte Carlo configuration was performed. For each site occupancy density, the Brownian dynamics simulations were run for a total of 2000 time steps to account for pinwheel rearrangements and reorganizations on the surface. In our Brownian dynamics simulation one time step is equivalent to the diffusion time for a pinwheel to travel a distance equal to the leg length a. The integration time step is set to $\Delta t = 0.0001$, which is sufficiently small to resolve local elastic relaxation processes and ensure stability of the simulation. This time step is approximately equal to 40 microseconds in real time, leading to the total simulation time of 80 milliseconds in real time for each Brownian dynamics simulation after the Monte Carlo initialization.

The final configuration from the Monte Carlo and Brownian dynamics simulations acts as input to determine the shear

modulus of the simulated clathrin network. To determine the shear modulus we impose (i) a uniform in-plane deformation to the network by applying constant displacement $\delta \sim 0.1a$ along the edges of the simulation box in the horizontal and vertical directions, and (ii) subject the network to uniform extension in the x and y direction separately. After finding the minimum-energy configuration for each displacement, the minimized energy *versus* displacements provides a quadratic-order relationship between energy and lattice strains, thus resulting in linear relationships between stresses and strains. The proportionality constants in these relationships give the storage and shear moduli.[54]

The stretching modulus κ_s was varied to approximate the modulus magnitude range shown in Fig. 4, while the bending modulus κ_b was chosen from previous clathrin network structure data.[46] A good fit is obtained using stretching modulus $k_BTa^2\kappa_s = 268$ and bending modulus $k_BT\kappa_b = 36$. For each occupancy density, we calculated the shear storage modulus (red diamonds) shown in Fig. 4 by averaging over 10 simulations. To determine each of the occupancies the same method was employed for the pure-percolation model, $\Delta\pi/\Delta\pi_{max}$ (eqn (2)). Fig. 4 demonstrates that the pinwheel model is capable of predicting the effective storage modulus of the clathrin network very well. It also illustrates the onset of an elastic percolating network corresponding to the rise of effective storage modulus followed by saturation of the elastic modulus at the maximum site occupancy.

Fig. 5b (left to right, top to bottom) illustrates snapshots obtained from Brownian dynamics simulations after 2000 steps for various occupancy densities between $\rho = 0.20$ and 0.98. In these snapshots, red circles are the hubs of clathrin proteins modeled by the pinwheels, solid black lines are bound legs, dashed blue lines are free (unbound) legs, and dashed blue circles indicate free pinwheels which have not bound to any other pinwheel.

Bond percolation theory states that above 65% site occupancy for a hexagonal lattice should create a spanning network. This is clearly seen from the snapshot taken at an occupancy density $\rho = 0.7$ (Fig. 5b), which is slightly above the percolation threshold, demonstrating cluster spanning in both horizontal and vertical directions.

The Monte Carlo simulation of depleted networks shows a gradual increase in network modulus, in contrast to the percolation model, but agrees with the experimental ISR data (Fig. 4). This gradual rise is due to the clustering of clathrin triskelia on the lipid surface into areas of concentrated clathrin density, which also causes the modulus to change slightly *below* 65% percolation (Fig. 4b).

Below $\rho = 0.85$ (Fig. 4b), our model predicted the modulus increase to be slightly shallower than was measured. Between $\rho = 0.85$–0.90, however, we predicted a sharper modulus increase than occurred. This transition occurred when the clathrin modulus was rising at its fastest rate. Since our Monte Carlo model does not model dynamic network formation, but only steady-state networks at discrete percolation densities, it is possible that network growth is kinetically limited at this point. Similar networks are also known to require time to age and strengthen, even after surface adsorption is finished.[55]

We note that the experimental measurements of dynamic modulus *versus* frequency (see Fig. S2†) suggest the network is composed of long-lived bonds over three decades on time for a mature lattice, which is consistent with the assembly being solid and unaffected by major reorganization processes at experimental time scales. Clathrin assembly in solution exhibits complex kinetic pathways for assembly marked by large scale reorganization of aggregates and cages over the course of hours to days.[33] However, these reorganization processes most likely influence 3D assembly due to the prevalence of aggregates and cages that arise under these conditions. The pair potentials and binding affinities used in the model also affect the shape of the modulus curve, and tuning these parameters could result in a better fit to the ISR data, although these parameters were chosen to match the pattern of clathrin network bond structures formed *in vivo*,[46] so large alterations could lead to unphysical results.

Above $\rho = 0.90$ the ISR data are no longer smooth and continuous due to the small oscillation amplitudes. This makes it difficult to draw strong conclusions about the relationship between the ISR data and the Monte Carlo model, but the general trends continue to match quite well. It is worth noting that the modulus obtained from Monte Carlo model asymptotically approaches its final modulus at very high densities, which contrasts with the pure percolation model (Fig. 4b).

In order to remove the kinetic issues associated with network growth, we also monitored clathrin adsorption and network growth during a series of discrete clathrin injections into the subphase, allowing the system to reach equilibrium between each injection. Using this procedure to test clathrin adsorption (Fig. 1), the first injection of protein resulted in the largest surface pressure increase, with each subsequent injection resulting in monotonically smaller surface pressure increases. However, serial clathrin injections do not produce a similar trend in modulus increase (Fig. 6, S4†). Rather, increasing clathrin concentrations result in a sigmoidal modulus increase, where initial clathrin injections increase the surface modulus very little, additional injections increase it substantially, and further injections again result in small increases. This sequence of small–large–small surface pressure increases is visible in

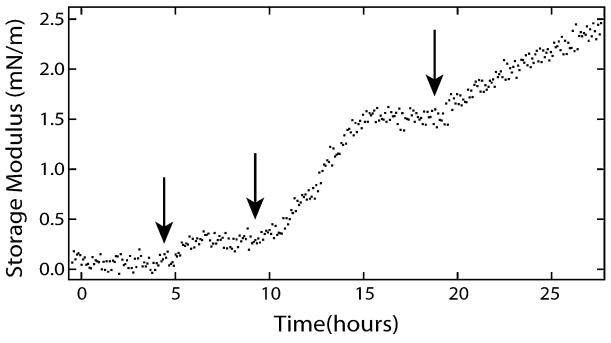

Fig. 6 The rise in surface modulus from serial clathrin injections follows a percolation type pattern. This contrasts with the pattern of surface pressure increase (Fig. 1, S4†). Arrows indicate the times of clathrin injection into the subphase.

Fig. 6 and is indicative of percolation network formation, where a critical surface density is required before a spanning network forms, and a global modulus change occurs. The data from Fig. 1 and 6 are directly compared in Fig. S4,† where the rise in surface pressure is concave, and the rise in surface modulus is convex. These data demonstrate that kinetic limitations in network growth are not responsible for the percolation-like behaviour of the network modulus increase in Fig. 4. Although the surface pressure can stabilize a few minutes after protein injection, a stable surface modulus can take many hours. Because of this, we were limited to only a few clathrin injections before experimental drift affected the measurements too strongly.

The large modulus variations in the ISR data are common when the clathrin networks gain rigidity, as the network is sensitive to strain, and measuring the network can damage it. Normally, the failure mode of adsorbed bio-interfaces *in vitro* is the slow desorption or oxidation of the agents. This occurs as a slow, continuous process, similar to the adsorption step. However, the failure mode of these clathrin networks is accompanied by sudden drops in the modulus, which is indicative of mechanical tearing, not protein desorption (Fig. S5†). Our inability to measure the stable formation of a complete clathrin network is directly related to our need to perturb it in order to measure it. Measuring at 0.5% strain allowed network formation to advance much farther than measuring at 2% strain before network tearing occurs (Fig. S5†). Strain sweeps on mature clathrin networks showed that network damage begins at strains approaching 0.2% (Fig. S6†), below which the data signal is too noisy to be useful. This implies that despite our use of the ISR at its technical limits, we were likely damaging the clathrin network after it began to percolate. It is possible that other rheology measurement systems which exert a smaller force over a smaller strain range (such as particle tracking based micro-rheology) can extend the range of the rheology measurements presented here.

In the absence of proteins that initiate endocytosis, clathrin seems to create large networks on a lipid monolayer, which acts as a cell membrane mimic. These clathrin networks appear to be temporally stable, but tear when exposed to shear strains above ~2%. The formation of the networks can be roughly approximated by simple percolation theory, but accurate modelling requires simulation, due to clathrin recruitment and self-association. Our Monte Carlo simulations seem to accurately track the growth of network mechanics, but further work still needs to be done to capture the kinetics of network formation and rearrangement.

Conclusions

We have demonstrated a method for monitoring the assembly of spanning, 2-dimensional clathrin lattices on lipid monolayers stabilized at the air–water interface. We used surface rheological techniques to follow the growth of the protein networks through mechanical changes of the lipid surface as the film forms. By using the increase in surface pressure to determine the amount of protein on the surface, and using Monte Carlo and Brownian dynamics simulations to capture the growing strength of the protein network as it forms, we can separate adsorption and network formation. This is the first attempt to monitor dynamic 2-dimensional clathrin network self-assembly, and is a step towards understanding assembly over a large parameter space, eventually developing a phase diagram for structural assembly based on mechanical models. These new insights into protein assembly can aid in the engineering of bio-inspired nano-assembly systems.

Experimental

Materials

Lipids were obtained from Avanti Polar Lipids (Alabaster, AL) and all buffers and salts were from Sigma Aldrich. Solvents were obtained from Sigma Aldrich, were of at least ACS grade, and were used without further purification, except for chloroform, which was distilled before use. Clathrin and adaptor proteins were isolated from bovine brain tissue using differential centrifugation and size exclusion chromatography as previously reported.[56] Bovine brain tissue was obtained from Harris Ranch (Coalinga, CA) and Innovative-Research (Novi, MI). Lipids were handled only with glass, stainless steel, and PTFE. The subphase was HKM buffer (25 mM Hepes pH 7.4, 125 mM potassium acetate, 5 mM magnesium acetate, 1 mM dithiothreitol) and the lipid monolayer was 20% PIP_2, 10% cholesterol, 35% SOPC, and 35% SOPE, and was used within one day of being prepared. All experiments were performed in either a cleanroom or a dust exclusion cabinet.

Interfacial shear rheology

All surface rheology experiments were performed in the lab of Gerry Fuller at Stanford University. Data for Fig. 2, 6, S1, S3 and S4† was obtained with a du Noüy ring in conjunction with a custom milled PTFE double couette dish and an ARG2 rheometer (TA Instruments, New Castle, DE) following techniques and equipment previously developed.[57] The subphase for these experiments was not stirred. Protein injection was done with glass syringes (Hamilton Company, Reno, NV), and a programmable syringe pump (New Era Pump Systems Inc., Farmingdale, NY).

All other surface rheology data was obtained with a custom built Interfacial Shear Rheometer (ISR) built on a Langmuir–Blodgett trough (KSV-NIMA, Finland). The trough subphase was mixed with a peristaltic pump. Data for Fig. 1 was obtained with a custom milled Teflon dish with a magnetically stirred subphase.

Starting lipid surface pressures (10 mN m^{-1}) were obtained by depositing the lipids in the gas phase and compressing the surface area for experiments using the ISR (Fig. 3, 4, S2, S5, and S6†). For other experimental setups (Fig. 1, 2, 6, S1, S3, and S4†) the initial lipid surface pressure was obtained by directly depositing the necessary amount of lipids needed to reach 10 mN m^{-1}, which was determined through pressure–area isotherm experiments. Protein was injected into the ISR subphase from behind the Langmuir–Blodgett trough barriers,

and into other PTFE dish subphases through holes drilled into the dish sidewalls.

Acknowledgements

We would like to thank the Gerry Fuller lab for the use of the ISR rheometry equipment and invaluable discussions, especially Michael Maas and Danielle Leiske. Additional thanks for assistance with surface experiments to Michael Toney and Chad Miller of SLAC, Ivan Kuzmenko and Binhua Lin of Argonne APS, and Jason Fabbri. This work was supported by the Department of Energy Office of Basic Energy Sciences, Materials Sciences and Engineering Division, under contract DE-AC02-76SF00515.

Notes and references

1 T. H. LaBean and H. Li, Constructing novel materials with DNA, *Nano Today*, 2007, **2**, 26–35.
2 S. H. Park, *et al.* Finite-Size, Fully Addressable DNA Tile Lattices Formed by Hierarchical Assembly Procedures, *Angew. Chem.*, 2006, **118**, 749–753.
3 S. H. Park, M. W. Prior, T. H. LaBean and G. Finkelstein, Optimized fabrication and electrical analysis of silver nanowires templated on DNA molecules, *Appl. Phys. Lett.*, 2006, **89**, 033901.
4 S. H. Park, *et al.* Programmable DNA self-assemblies for nanoscale organization of ligands and proteins, *Nano Lett.*, 2005, **5**, 729–733.
5 S. Behrens, J. Wu, W. Habicht and E. Unger, Silver nanoparticle and nanowire formation by microtubule templates, *Chem. Mater.*, 2004, **16**, 3085–3090.
6 S. Lagziel-Simis, N. Cohen-Hadar, H. Moscovich-Dagan, Y. Wine and A. Freeman, Protein-mediated nanoscale biotemplating, *Curr. Opin. Biotechnol.*, 2006, **17**, 569.
7 N. Cohen-Hadar, *et al.* Monitoring the stability of crosslinked protein crystals biotemplates: A feasibility study, *Biotechnol. Bioeng.*, 2006, **94**, 1005–1011.
8 T. Scheibel, *et al.* Conducting nanowires built by controlled self-assembly of amyloid fibers and selective metal deposition, *Proc. Natl. Acad. Sci. U. S. A.*, 2003, **100**, 4527–4532.
9 M. Bergkvist, S. S. Mark, X. Yang, E. R. Angert and C. A. Batt, Bionanofabrication of ordered nanoparticle arrays: effect of particle properties and adsorption conditions, *J. Phys. Chem. B*, 2004, **108**, 8241–8248.
10 S. S. Mark, *et al.* Thin film processing using S-layer proteins: biotemplated assembly of colloidal gold etch masks for fabrication of silicon nanopillar arrays, *Colloids Surf., B*, 2007, **57**, 161–173.
11 S. S. Mark, M. Bergkvist, X. Yang, E. R. Angert and C. A. Batt, Self-assembly of dendrimer-encapsulated nanoparticle arrays using 2-D microbial S-layer protein biotemplates, *Biomacromolecules*, 2006, **7**, 1884–1897.
12 S. S. Mark, *et al.* Bionanofabrication of metallic and semiconductor nanoparticle arrays using S-layer protein lattices with different lateral spacings and geometries, *Langmuir*, 2006, **22**, 3763–3774.
13 F. Zhang, *et al.* Clathrin adaptor GGA1 polymerizes clathrin into tubules, *J. Biol. Chem.*, 2007, **282**, 13282–13289.
14 K. T. Nam, B. R. Peelle, S.-W. Lee and A. M. Belcher, Genetically driven assembly of nanorings based on the M13 virus, *Nano Lett.*, 2004, **4**, 23–27.
15 S. Brumfield, *et al.* Heterologous expression of the modified coat protein of Cowpea chlorotic mottle bromovirus results in the assembly of protein cages with altered architectures and function, *J. Gen. Virol.*, 2004, **85**, 1049–1053.
16 M. Knez, *et al.* Biotemplate synthesis of 3 nm nickel and cobalt nanowires, *Nano Lett.*, 2003, **3**, 1079–1082.
17 S.-Y. Lee, E. Royston, J. N. Culver and M. T. Harris, Improved metal cluster deposition on a genetically engineered tobacco mosaic virus template, *Nanotechnology*, 2005, **16**, S435.
18 C. Liu, *et al.* Magnetic viruses via nano-capsid templates, *J. Magn. Magn. Mater.*, 2006, **302**, 47–51.
19 C. Radloff, R. A. Vaia, J. Brunton, G. T. Bouwer and V. K. Ward, Metal nanoshell assembly on a virus bioscaffold, *Nano Lett.*, 2005, **5**, 1187–1191.
20 R. Tsukamoto, M. Muraoka, M. Seki, H. Tabata and I. Yamashita, Synthesis of CoPt and $FePt_3$ nanowires using the central channel of tobacco mosaic virus as a biotemplate, *Chem. Mater.*, 2007, **19**, 2389–2391.
21 K. T. Nam, *et al.* Virus-enabled synthesis and assembly of nanowires for lithium ion battery electrodes, *Science*, 2006, **312**, 885–888.
22 J. Heuser and T. Kirchhausen, Deep-etch views of clathrin assemblies, *J. Ultrastruct. Res.*, 1985, **92**, 1–27.
23 P. K. Sorger, R. A. Crowther, J. T. Finch and B. M. Pearse, Clathrin cubes: an extreme variant of the normal cage, *J. Cell Biol.*, 1986, **103**, 1213–1219.
24 B. Falkowska-Hansen, M. Falkowski, P. Metharom, D. Krunic and S. Goerdt, Clathrin-coated vesicles form a unique net-like structure in liver sinusoidal endothelial cells by assembling along undisrupted microtubules, *Exp. Cell Res.*, 2007, **313**, 1745–1757.
25 J. E. Heuser, J. H. Keen, L. M. Amende, R. E. Lippoldt and K. Prasad, Deep-etch visualization of 27S clathrin: a tetrahedral tetramer, *J. Cell Biol.*, 1987, **105**, 1999–2009.
26 T. Yoshimura, K. Kameyama, S. Maezawa and T. Takagi, Skeletal structure of clathrin triskelion in solution: experimental and theoretical approaches, *Biochemistry*, 1991, **30**, 4528–4534.
27 M. L. Ferguson, *et al.* Conformation of a clathrin triskelion in solution, *Biochemistry*, 2006, **45**, 5916–5922.
28 R. Nossal, Energetics of clathrin basket assembly, *Traffic*, 2001, **2**, 138–147.
29 B. M. Pearse, C. J. Smith and D. J. Owen, Clathrin coat construction in endocytosis, *Curr. Opin. Struct. Biol.*, 2000, **10**, 220–228.
30 J. Lipfert and S. Doniach, Small-angle X-ray scattering from RNA, proteins, and protein complexes, *Annu. Rev. Biophys. Biomol. Struct.*, 2007, **36**, 307–327.
31 B. Alberts, *et al.*, *Molecular Biology of the Cell*, Garland Science, 2002.
32 M. G. Ford, *et al.* Curvature of clathrin-coated pits driven by epsin, *Nature*, 2002, **419**, 361–366.

33 A. P. Schoen, *et al.* Dynamic remodeling of disordered protein aggregates is an alternative pathway to achieve robust self-assembly of nanostructures, *Soft Matter*, 2013, **9**, 9137–9145.
34 M. G. Ford, *et al.* Simultaneous binding of PtdIns (4, 5) P2 and clathrin by AP180 in the nucleation of clathrin lattices on membranes, *Science*, 2001, **291**, 1051–1055.
35 H. Brockman, Lipid monolayers: why use half a membrane to characterize protein-membrane interactions?, *Curr. Opin. Struct. Biol.*, 1999, **9**, 438–443.
36 C. F. Brooks, G. G. Fuller, C. W. Frank and C. R. Robertson, An interfacial stress rheometer to study rheological transitions in monolayers at the air-water interface, *Langmuir*, 1999, **15**, 2450–2459.
37 S. Reynaert, C. F. Brooks, P. Moldenaers, J. Vermant and G. G. Fuller, Analysis of the magnetic rod interfacial stress rheometer, *J. Rheol.*, 2008, **52**, 261.
38 L. D. Mayer, G. L. Nelsestuen and H. L. Brockman, Prothrombin association with phospholipid monolayers, *Biochemistry*, 1983, **22**, 316–321.
39 H. S. Moskowitz, C. T. Yokoyama and T. A. Ryan, Highly cooperative control of endocytosis by clathrin, *Mol. Biol. Cell*, 2005, **16**, 1769–1776.
40 J. Majewski, T. L. Kuhl, K. Kjaer and G. S. Smith, Packing of ganglioside-phospholipid monolayers: an X-ray diffraction and reflectivity study, *Biophys. J.*, 2001, **81**, 2707–2715.
41 F. Monroy, F. Ortega, R. G. Rubio, H. Ritacco and D. Langevin, Surface rheology of two-dimensional percolating networks: Langmuir films of polymer pancakes, *Phys. Rev. Lett.*, 2005, **95**, 056103.
42 C. W. Macosko, *Rheology: principles, measurements, and applications*, Wiley-VCH, Inc., 1994.
43 D. Boal, *Mechanics of the Cell*, Cambridge University Press, 2012.
44 J. G. Zabolitzky, D. J. Bergman and D. Stauffer, Precision calculation of elasticity for percolation, *J. Stat. Phys.*, 1986, **44**, 211–223.
45 D. Stauffer & A. Aharony, *Introduction to Percolation Theory*, Taylor and Francis, 1994.
46 S. Mehraeen, N. Cordella, J. S. Yoo and A. J. Spakowitz, Impact of defect creation and motion on the thermodynamics and large-scale reorganization of self-assembled clathrin lattices, *Soft Matter*, 2011, **7**, 8789–8799.
47 N. Cordella, T. J. Lampo, S. Mehraeen and A. J. Spakowitz, Membrane Fluctuations Destabilize Clathrin Protein Lattice Order, *Biophys. J.*, 2014, **106**, 1476–1488.
48 W. K. Den Otter, M. R. Renes and W. J. Briels, Self-assembly of three-legged patchy particles into polyhedral cages, *J. Phys.: Condens. Matter*, 2010, **22**, 104103.
49 W. K. Den Otter, M. R. Renes and W. J. Briels, Asymmetry as the key to clathrin cage assembly, *Biophys. J.*, 2010, **99**, 1231–1238.
50 W. K. Den Otter and W. J. Briels, The generation of curved clathrin coats from flat plaques, *Traffic*, 2011, **12**, 1407–1416.
51 R. Matthews and C. N. Likos, Influence of Fluctuating Membranes on Self-Assembly of Patchy Colloids, *Phys. Rev. Lett.*, 2012, **109**, 178302.
52 R. Matthews and C. N. Likos, Structures and pathways for clathrin self-assembly in the bulk and on membranes, *Soft Matter*, 2013, **9**, 5794–5806.
53 K. Binder & D. W. Heermann, *Monte Carlo simulation in statistical physics: an introduction*, Springer, 2010.
54 L. D. Landau & E. M. Lifshitz, *Elasticity Theory*, Butterworth-Heinemann, 1986.
55 G. G. Fuller, Rheology of mobile interfaces, *Rheol. Rev.*, 2003, 77–124.
56 A. P. Jackson, *Biomembrane Protocols: I. Isolation and Analysis*, Humana Press, Inc., 1993, vol. 19.
57 S. Vandebril, A. Franck, G. G. Fuller, P. Moldenaers and J. Vermant, A double wall-ring geometry for interfacial shear rheometry, *Rheol. Acta*, 2010, **49**, 131–144.